Single-shot and measurement-based quantum error correction via fault complexes

Letter

Single-shot and measurement-based quantum error correction via fault complexes

Timo Hillmann,[1,2,*] Guillaume Dauphinais,[1] Ilan Tzitrin,[1,†] and Michael Vasmer[1,3,4]

[1]*Xanadu Quantum Technologies Inc., Toronto, Ontario M5G 2C8, Canada*

[2]*Department of Microtechnology and Nanoscience (MC2), Chalmers University of Technology, SE-412 96 Gothenburg, Sweden*

[3]*Perimeter Institute for Theoretical Physics, Waterloo, Ontario N2L 2Y5, Canada*

[4]*Institute for Quantum Computing, Waterloo, Ontario N2L 3G1, Canada*

(Received 11 November 2024; revised 22 April 2025; accepted 16 September 2025; published 9 October 2025)

Photonics provides a viable path to a scalable fault-tolerant quantum computer. The natural framework for this platform is measurement-based quantum computation, where fault-tolerant graph states supersede traditional quantum error-correcting codes. However, the existing formalism for foliation—the construction of fault-tolerant graph states—does not reveal how certain properties, such as single-shot error correction, manifest in the measurement-based setting. We introduce the fault complex, a representation of dynamic quantum error-correction protocols particularly well suited to describe foliation. Our approach enables precise computation of fault tolerance properties of foliated codes and provides insights into circuit-based quantum computation. Analyzing the fault complex yields improved thresholds for three- and four-dimensional toric codes, a generalization of stability experiments, and the existence of single-shot lattice surgery with higher-dimensional topological codes.

DOI: 10.1103/cjb4-l57n

Introduction. Photonic platforms for quantum computing [1–6] are well suited to measurement-based quantum computing (MBQC) [7]. In this paradigm, in contrast to circuit-based quantum computation (CBQC), the central object is not a quantum error-correcting (QEC) code but a fault-tolerant graph state (FTGS). Various methods for constructing FTGS exist [8–10], with the concept of foliation [11,12] offering a prescription for any Calderbank-Shor-Steane (CSS) code [13,14]. Here, we introduce the *fault complex*, a representation of faults in a dynamic QEC protocol (rather than a static QEC code) formulated in the language of homology and chain complexes [15–18]. We focus on fault complexes obtained via foliation, which we recast in the language of homology as a tensor product [19,20] between a CSS code and a repetition code. This formalism allows us to easily calculate properties like the fault distance and also applies to CBQC, where it represents repeated rounds of error correction. Analysis of the fault complex enables us to understand the decoding of single-shot codes in MBQC and achieve improved error thresholds for three-dimensional (3D) and 4D toric codes [21–24]. Through the explicit calculation of the homology groups of the fault complex, we generalize the notion of stability experiments [25], which in turn allows us to conclude that single-shot lattice surgery is possible in higher-dimensional topological codes. The fault complex provides a formal language for fault-tolerant protocols, similar to how homological descriptions serve CSS codes, laying the groundwork for future advances in fault-tolerant quantum computation.

Background and notation. An $[n, k, d]$ binary linear code C forms a k-dimensional subspace within the n-dimensional vector space over $\mathbb{F}_2$. Such a code can be defined by a parity-check matrix (PCM) H, where the codewords are the elements of $\ker H$. The distance d is the minimum Hamming weight of any nonzero codeword. We use e_i to denote the ith unit vector and $[M]_j$ to denote the jth row of a matrix M. We write $\mathbf{0}$ and $\mathbf{1}$ for the all-zero and all-one vectors, respectively.

A stabilizer code [26] is the quantum analog of a linear code and is defined by an Abelian subgroup, $\mathcal{S}$, of the Pauli group with $-I \notin \mathcal{S}$. The codespace is the $+1$ eigenspace of $\mathcal{S}$; logical operators commute with $\mathcal{S}$ but are not themselves in $\mathcal{S}$. The notation $[\![n, k, d]\!]$ describes a code in which the stabilizer group is generated by $m = n - k$ independent generators, which are themselves elements of the n-qubit Pauli group $\mathcal{P}_n$. The number of encoded qubits is k and the distance d is determined by the minimum weight nontrivial logical operator. A stabilizer code admitting a set of stabilizer generators that are each either X-type or Z-type operators is referred to as a CSS code [13,14]. These codes can be described by two classical binary linear codes with PCMs H_X and H_Z representing stabilizer generators as tensor products of X and I, and Z and I, respectively. Commutativity of X- and Z-type generators is expressed through the condition $H_Z^T H_X = 0$. Error correction proceeds via the measurement of the stabilizer generators, yielding the syndrome s, which is the list of stabilizer eigenvalues. This allows the detection and correction of Pauli errors that anticommute with stabilizer

*Contact author: timo.hillmann@rwth-aachen.de

†Contact author: ilan@xanadu.ai

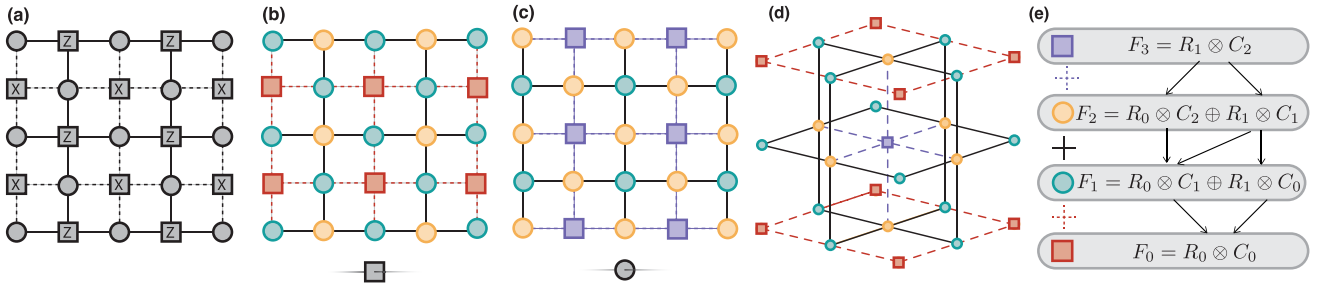

FIG. 1. Foliation of the surface code viewed as a fault complex. (a) The distance-3 surface code Tanner graph with circles representing qubits, squares representing X and Z checks, and dashed and solid lines representing the connectivity of these checks, respectively. (b), (c) Hypergraph product of (a) with a repetition code check and bit node, respectively. This yields two types of fault locations, teal and yellow, along with primal (red) and dual (purple) detectors. Dashed and solid lines indicate boundary maps of the fault complex. For simplicity, we omit out-of-plane connections. (d) Unit cell of the fault complex obtained by stacking alternating layers of (b) and (c). A dual detector (purple) is formed by the parity of six dual fault locations (yellow). Vertical red dashed lines are omitted for clarity. (e) Mathematical structure of the fault complex and its relation to (b)–(d): colored circles and squares represent chain complex vector spaces and lines represent boundary maps.

generators; a classical decoder is used to infer recovery operators given a syndrome.

Here, a chain complex of length n denotes a collection of $\mathbb{F}_2$-vector spaces C_i and linear maps ∂_i^C called boundary operators,

$$\mathcal{C} = \{0\} \xrightarrow{\partial_{n+1}^C} C_n \xrightarrow{\partial_n^C} \cdots \xrightarrow{\partial_2^C} C_1 \xrightarrow{\partial_1^C} C_0 \xrightarrow{\partial_0^C} \{0\}, \tag{1}$$

with the composition fulfilling $\partial_i^C \partial_{i+1}^C = 0$. We suppress superscripts if no distinction is necessary. The quotient $H_i(\mathcal{C}) := \ker \partial_i / \mathrm{im}\, \partial_{i+1}$ is called the ith homology group of $\mathcal{C}$. Associated with $\mathcal{C}$ is also a cochain complex, with coboundary operators $\delta^i : C_i \to C_{i+1}$ defined as $\delta^i = \partial_{i+1}^T$:

$$\mathcal{C}^T = \{0\} \xrightarrow{\delta^{-1}} C_0 \xrightarrow{\delta^0} C_1 \cdots \xrightarrow{\delta^{n-1}} C_n \xrightarrow{\delta^n} \{0\}, \tag{2}$$

with cohomology groups $H^i := \ker \delta^i / \mathrm{im}\, \delta^{i-1}$.

Each length-1 chain complex describes an $[n, k, d]$ linear code with boundary map $\partial_1 = H$ from $\mathbb{F}_2^n$ to the space of syndromes $\mathbb{F}_2^r$ with $r \geqslant n - k$. Similarly, a CSS code, $\mathcal{C}$, can represented by a length-2 chain (sub)complex

$$\cdots \to C_{i+1} \xrightarrow{\partial_{i+1}} C_i \xrightarrow{\partial_i} C_{i-1} \to \cdots, \tag{3}$$

where, by convention, $\partial_{i+1} = H_Z^T$ and $\partial_i = H_X$, such that $\partial_i \partial_{i+1} = 0$ is encoded in the condition that $H_X H_Z^T = 0$. Identifying qubits with the space C_i, the code parameters are $n = \dim C_i$, $k = \dim H_i(\mathcal{C})$, and the logical operators are elements of the groups $H_i(\mathcal{C})$ and $H^i(\mathcal{C})$, with the smallest weight element defining d.

Motivating example. A common way to obtain an FTGS from a CSS code is via foliation [11]. In this procedure, the X and Z Tanner graphs of the code are interpreted as alternating layers of the FTGS and data qubits between adjacent layers are entangled with each other; see Figs. 1(a)–1(d). The computation is then performed by a sequence of adaptive local measurements on the FTGS. We observe that foliation can be algebraically formulated as the tensor (or hypergraph [19,20]) product of a base CSS code with a repetition code [27]; see Fig. 1(e). Denote the resulting complex as $\mathcal{F} = \mathcal{C} \times \mathcal{R}$, where $\mathcal{C}$ is a length-2 chain complex describing a CSS code and $\mathcal{R}$ is a chain complex describing a repetition code. The spaces of $\mathcal{F}$ are

$$F_j = \bigoplus_{\ell+m=j} R_\ell \otimes C_m, \tag{4}$$

where R_ℓ and C_m are the ℓth and mth spaces of $\mathcal{R}$ and $\mathcal{C}$, respectively. The boundary operators of $\mathcal{F}$ are

$$\partial_j = \left(\begin{array}{c|c} \mathbb{1}_r \otimes \partial_j^C & R \otimes \mathbb{1}_{n_{j-1}^C} \\ \hline 0 & \mathbb{1}_c \otimes \partial_{j-1}^C \end{array}\right), \tag{5}$$

where ∂_j^C is the jth boundary operator of $\mathcal{C}$ and R is the $r \times c$ PCM of the binary linear code. One can observe that ∂_2 is the biadjacency matrix of the (bipartite) FTGS, whereas ∂_1 and ∂_3^T describe the detectors (or foliated stabilizers) of the FTGS. For example, the rows of ∂_1 are of the form $(e_\alpha \otimes [H_X]_\beta | [R]_\alpha \otimes e_\beta)$, with an analogous form for the columns of ∂_3. These are exactly the foliated stabilizers of [11]; see Fig. 1(d), which illustrates a dual detector. Each detector (row) above is triggered by a fault on one of the qubits participating in the check $[H_X]_\beta$ or by a syndrome fault in an adjacent layer.

Fault complexes. Motivated by the previous example, we define a fault complex to be a length-3 chain (sub)complex $\mathcal{F}$,

$$\cdots \to F_{i+2} \xrightarrow{\partial_{i+2}} F_{i+1} \xrightarrow{\partial_{i+1}} F_i \xrightarrow{\partial_i} F_{i-1} \to \cdots, \tag{6}$$

where we define *primal fault locations* to be elements of F_i and *dual fault locations* to be elements of F_{i+1}. The fault complex has $n = n_i + n_{i+1}$ total faults, where $n_i = \dim F_i$. The boundary map ∂_{i+1} determines equivalent primal and dual faults. We define the primal and dual *detector matrices* to be $D_X = \partial_i$ and $D_Z = \partial_{i+2}^T$, respectively. The syndrome of a primal fault $x \in F_i$ is $D_X x$ and the support of a primal detector $u \in F_{i-1}$ is $D_X^T u$ and similarly for dual faults and detectors. In a fault complex, there is no requirement for the commutativity of the primal and dual detector matrices. Instead, we have $\partial_i \partial_{i+1} = 0$, meaning that a primal fault that is equivalent to a dual fault has trivial (primal) syndrome, with an analogous interpretation for $\partial_{i+2}^T \partial_{i+1}^T = 0$.

We refer to the elements of $H^i(\mathcal{F})$ and $H_{i+1}(\mathcal{F})$ as primal and dual *logical correlations*, respectively. These represent the information that the fault complex is designed to protect. Similarly, the elements of $H_i(\mathcal{F})$ and $H^{i+1}(\mathcal{F})$ are the primal

and dual *logical errors*, respectively. These operators change the values of the logical correlations but have no syndrome and are therefore undetectable. Note that the number of primal logical correlations (or errors) $k_i = \dim H^i(\mathcal{F}) = \dim H_i(\mathcal{F})$ need not equal the number of dual logical correlations (or errors) $k_{i+1} = \dim H_{i+1}(\mathcal{F}) = \dim H^{i+1}(\mathcal{F})$. The primal (dual) *fault distance* d_i (d_{i+1}) of the fault complex is the weight of the minimal weight primal (dual) logical error.

Recently, there have been many proposals for formalizing fault-tolerant protocols [9,10,28–35], some of which resemble our fault complexes. In particular, our definition of a fault complex builds on the definition of a *fault-tolerant cluster state* in [10]. We also note that fault complexes are distinct from the *fault-tolerant complexes* of [32], which are defined geometrically and are limited to topological codes. Fault complexes have an interpretation in CBQC where the faults can represent both qubit, gate, and measurement errors. In this interpretation, ∂_{i+1} is related to the gauge group of the space-time code; see [36] for further discussion. Here, we concentrate on the interpretation of fault complexes in MBQC.

Foliated CSS codes. We now return to our motivating example of the fault complex $\mathcal{F} = \mathcal{C} \times \mathcal{R}$, where $\mathcal{C}$ represents a CSS code and $\mathcal{R}$ represents a repetition code. Suppose that R, H_X, and H_Z are full rank. From the Künneth formula, we obtain the number of primal and dual correlations

$$k_i = \dim H_0(\mathcal{R}) \dim H_i(\mathcal{C}) + \dim H_1(\mathcal{R}) \dim H_{i-1}(\mathcal{C}),$$
$$k_{i+1} = \dim H_0(\mathcal{R}) \dim H_{i+1}(\mathcal{C}) + \dim H_1(\mathcal{R}) \dim H_i(\mathcal{C}).$$

One can show [20,36] that the primal and dual fault distances of $\mathcal{F}$ are given by

$$d_i = \min[d_0(\mathcal{R})d_i(\mathcal{C}), d_1(\mathcal{R})d_{i-1}(\mathcal{C})],$$
$$d_{i+1} = \min[d_0(\mathcal{R}^T)d_{i+1}(\mathcal{C}^T), d_1(\mathcal{R}^T)d_i(\mathcal{C}^T)], \tag{7}$$

where $d_i(\mathcal{C})$ and $d_i(\mathcal{C}^T)$ are equal to the minimal weight of an element in $H_i(\mathcal{C})$ and $H^i(\mathcal{C})$, respectively. For trivial homology groups the associated distance is defined as ∞.

The logical correlations of $\mathcal{F}$ are recovered from the homology group; that is, for example,

$$H_2(\mathcal{F}) \cong H_0(\mathcal{R}) \otimes H_2(\mathcal{C}) \oplus H_1(\mathcal{R}) \otimes H_1(\mathcal{C})$$
$$= \left\langle (\mathbf{0}, \mathbf{1} \otimes \ell_Z) \mid \ell_Z \in \ker H_X / \mathrm{im}\, H_Z^T \right\rangle, \tag{8}$$

where ℓ_Z is a logical Z operator of the base code. See [36] for a detailed derivation. This operator is a dual logical correlation; it acts as a copy of the logical Z operator on the qubits in the $R_1 \otimes C_1$ block of the F_1 space. The dual logical errors are given by

$$H^2(\mathcal{F}) \cong H^0(\mathcal{R}) \otimes H^2(\mathcal{C}) \oplus H^1(\mathcal{R}) \otimes H^1(\mathcal{C})$$
$$= \left\langle (\mathbf{0}, (1, 0, \ldots, 0) \otimes \ell_X) \mid \ell_X \in \ker H_Z / \mathrm{im}\, H_X^T \right\rangle, \tag{9}$$

where ℓ_X is a logical X operator of the base code. We observe that this operator acts as a logical X operator on one of the factors in the $R_1 \otimes C_1$ portion of the F_1 space. Applying Eq. (7), we find that the (dual) fault distance of $\mathcal{F}$ is $d_2 = d_X$—the X distance of the base code.

For our choice of $\mathcal{R}$, the homology groups $H_0(\mathcal{R})$ and $H^0(\mathcal{R})$ are trivial, so the fault complex lacks primal logical correlations arising from the base code's logical X. This may seem surprising, given that the foliated surface code can be used to prepare an encoded Bell state on the two boundaries [37]. There is no contradiction, however: the interpretation of fault complexes as foliated codes implicitly assumes that all qubits are measured in the X basis during the protocol and therefore that the encoded Bell state of [37] is measured destructively. The analogous CBQC interpretation is of a memory experiment with logical state preparation and readout both performed in the Z basis. In addition, we note that all the logical correlations can be recovered by considering an alternative repetition code PCM; see [36].

Stability experiments. Lattice surgery [38] is the leading technique for performing logical operations on topological codes [39,40] and stability experiments [25] estimate the logical error during a lattice surgery operation. Such experiments test our ability to accurately measure the product of many stabilizer generators.

Returning to our foliated CSS code example, suppose that H_X of the base code $\mathcal{C}$ is rank deficient. The fault complex $\mathcal{F} = \mathcal{R} \times \mathcal{C}$ now has additional logical correlations and errors coming, respectively, from the following homology groups:

$$H^1(\mathcal{F}) \cong \left\langle (\mathbf{0}, (1, 0, \ldots, 0) \otimes g) \mid g \in \ker H_X^T \right\rangle,$$
$$H_1(\mathcal{F}) \cong \langle (\mathbf{0}, \mathbf{1} \otimes h) \mid h \in C_0/\mathrm{im}\, H_X \rangle. \tag{10}$$

Here, g represents any subset of H_X rows that sum to zero and h is any vector in C_0 that is not the syndrome of a Z-type error. An example of such a code is a 2D surface code with four smooth boundaries; in this case we have $g = \mathbf{1}$ (the product of all X stabilizers is I) and $h = (1, 0, \ldots, 0)$ (all valid syndromes have even weight). The logical correlation g is exactly the product of stabilizer generators considered in stability experiments. Using Eq. (7) we find that the primal distance of $\mathcal{F}$ is $d_1 = \delta$, i.e., equal the distance of the repetition code (or the number of CBQC measurement rounds; cf. [25]). A 2D surface code with four smooth boundaries encodes no logical qubits, but if instead we let $\mathcal{C}$ be the 2D toric code (with periodic boundaries) then our formalism shows that the fault complex $\mathcal{F} = \mathcal{R} \times \mathcal{C}$ can be used to perform a combined memory and stability experiment; see [36].

Single-shot lattice surgery. Certain CSS codes are naturally associated with length-3 or length-4 chain complexes, where the additional vector spaces represent metachecks, i.e., redundancies between subsets of checks. Metachecks are related to single-shot error correction [23,41,42], where a single round of parity-check measurements suffices for fault-tolerant QEC.

As a prototypical example of a code with metachecks, let $\mathcal{C}$ represent the 3D toric code [21,22] defined on an $L \times L \times L$ cubic tiling, which has single-shot QEC for Z errors. We focus on this code for ease of presentation, but our results also hold for true single-shot CSS codes such as the 4D toric code. We assign the metacheck matrix $M_X = \partial_1^C$ and PCMs $H_X = \partial_2^C$ and $H_Z = (\partial_3^C)^T$. The primal detectors of the fault complex $\mathcal{F} = \mathcal{R} \times \mathcal{C}$ are given by ∂_2, which now contains the metachecks; see [36] for the explicit expression. We note that $\mathcal{F}$ is effectively a length-3 chain complex exactly because

"data" and "measurement" faults are treated on an equal footing; see [36] for an extended discussion.

The expression for the primal logical correlations and errors of $\mathcal{F}$ is the same as Eq. (10), but now with $g \in \ker H_X^T / \mathrm{im}\, M_X^T$ and $h \in \ker M_X / \mathrm{im}\, H_X$. As in the previous example, g is the logical correlation relevant for stability experiments and lattice surgery and h is the logical error that can disrupt this correlation. In the 3D toric code, there are three independent choices of g given by all edges cutting through one of the independent 2D planes of the tiling. The corresponding h vectors correspond to noncontractible chains of edges along one of the coordinate axes of the tiling. As a result, all choices of h have extensive weight, i.e., $|h| \geqslant L$. Thus, even for a fault complex formed using a constant-length repetition code, a macroscopic number of faults ($\sim L$) is necessary to disrupt the g logical correlations. This is captured by the primal fault distance of $\mathcal{F}$, $d_1 = \delta L$, where $\delta = d_1(\mathcal{R})$ is the distance of the repetition code. Therefore, higher dimensional topological codes such as the 3D and 4D toric codes are compatible with *single-shot lattice surgery*, though at the cost of reduced performance. The full distance can be restored by choosing $\mathcal{R}$ such that $\delta = L = O(\sqrt{d})$ (where d is the distance of the code) or equivalently by performing $O(\sqrt{d})$ rounds of stabilizer measurement in the lattice surgery protocol. This should be contrasted with the 2D toric code case where the number of measurement rounds must be $O(d)$. Thus we expect that a fault-tolerant quantum computing architecture based on the 4D toric code would have an asymptotic space-time overhead reduction when compared to the standard 2D toric code architecture.

We address the case of single-shot codes with rank-deficient PCMs without metachecks in [36]. We note that there exist single-shot quantum codes with full-rank PCMs [43,44], to which our arguments above cannot be applied, and the existence of single-shot lattice surgery protocols for these codes remains an open question. We conjecture that codes enabling single-shot lattice surgery without performance degradation can be constructed from the balanced product of two good qLDPC codes [45–49].

Improved decoding of single-shot codes. Estimating the error threshold of a single-shot code requires simulating multiple rounds of noisy syndrome measurement until the threshold has converged [50]. Since in MBQC there always exist detectors spanning multiple rounds, decoding must proceed using an overlapping window decoder [21,51–54], which is naturally defined for a fault complex. The fault complex framework provides a systematic guide for constructing efficient simulations and evaluating the performance of these protocols.

A (w, c)-overlapping window decoder determines in each round a correction for a window of $w \in \mathbb{N}^+$ rounds and commits a correction to $c \leqslant w$ rounds; see Refs. [53,55] for a more detailed description. Here, one round constitutes a check node and a bit node layer; see Fig. 1. For the 3D toric code, the effective distance of the decoding window then becomes $\min(wL, L^2)$ [36]. However, wL is the weight of timelike logical errors and, in this section, we consider memory experiments, i.e., only spacelike logical errors cause logical failures; see [36] for stability experiment simulations. State-of-the-art

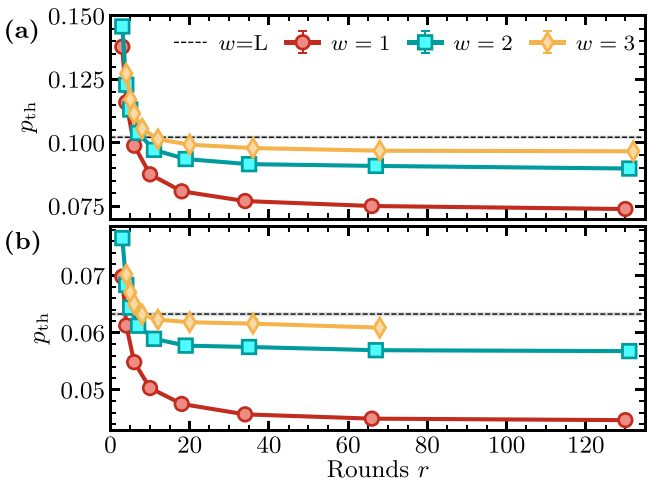

FIG. 2. Sustainable thresholds for 3D (a) and 4D (b) toric codes under phenomenological Pauli noise. Markers represent the threshold for a $(w, 1)$-overlapping window decoder as a function of noisy syndrome rounds. The black dashed line shows the threshold for the optimal window choice $w = L$; see [36] for details.

results in decoding higher-dimensional topological codes [24] employ a single-stage decoding approach that is recovered using a (1, 1)-overlapping window decoder [36]. We find that increasing w to 2 or 3 significantly increases the sustainable threshold of 3D and 4D toric codes compared to $w = 1$ when using belief propagation (BP) plus ordered statistics decoding (OSD) [56,57]; see [36] for details concerning the simulations. For $w = 3$, the thresholds for phenomenological Pauli noise (see [36] for a photonic noise model) of approximately 9.65% (3D) and 5.9% (4D) surpass all previous results [23,24,58–64], approaching the thresholds achieved with the optimal window choice $w = L$; see Fig. 2(a) and Fig. 2(b). We note that, for the 3D toric code, we only consider primal faults, as the dual side of the fault complex does not have the single-shot property.

While larger decoding regions increase decoding time, recent advances provide solutions. Findings on localized statistics decoding [65], a parallelizable OSD variant, and belief propagation for higher-dimensional toric codes [64] suggest time-efficient decoding with minimal performance reduction, supporting the practical applicability of our results.

Conclusion. We introduced fault complexes to represent dynamic QEC protocols and characterize foliated codes. This approach provided insights into stability experiments and lattice surgery and yielded improved decoding protocols for higher-dimensional topological codes like the 4D toric code. The increased thresholds and space-time overhead advantages make 4D toric codes promising for compatible architectures like photonics [1–6], trapped ions [66], and neutral atoms [67]. While algorithmic fault tolerance [68] offers a lower overhead, it requires complex decoding; 4D toric codes allow simpler windowed decoding. Meanwhile, the lower threshold requirements of 3D toric codes make them suitable for experimental validation in the near term.

Our formalism can extend to circuit-level noise by, for example, reformulating Li's [35] LDPC representation of

fault-tolerant quantum circuits [many of their results in [35, Sec. VIII] are already structurally equivalent to Eq. (5)]. Future work could explore the fault complexes of subsystem codes [69–71] (especially those with single-shot error correction [41,50,72]), symplectic chain complexes for non-CSS codes, and alternative product constructions like balanced [48] and lifted [73] products. In addition, by using alternative linear codes in the construction, we may hope to algebraically recover FTGS beyond foliation [9,32]. See [36] for some initial ideas on these extensions.

Acknowledgments. The authors would like to thank B. Brown, C. Chubb, A. Daniel, A. Pesah, T. Stace, A. Townsend-Teague, and D. Williamson for insightful discussions. We thank R. Alexander, J. E. Bourassa, and E. Sabo for feedback on an earlier draft of this manuscript. Research at Perimeter Institute is supported in part by the Government of Canada through the Department of Innovation, Science and Economic Development Canada and by the Province of Ontario through the Ministry of Colleges and Universities. Computations were performed on the Niagara supercomputer at the SciNet HPC Consortium. SciNet is funded by Innovation, Science and Economic Development Canada, the Digital Research Alliance of Canada, the Ontario Research Fund: Research Excellence, and the University of Toronto.

[1] J. E. Bourassa, R. N. Alexander, M. Vasmer, A. Patil, I. Tzitrin, T. Matsuura, D. Su, B. Q. Baragiola, S. Guha, G. Dauphinais, K. K. Sabapathy, N. C. Menicucci, and I. Dhand, Blueprint for a scalable photonic fault-tolerant quantum computer, Quantum **5**, 392 (2021).

[2] I. Tzitrin, T. Matsuura, R. N. Alexander, G. Dauphinais, J. E. Bourassa, K. K. Sabapathy, N. C. Menicucci, and I. Dhand, Fault-tolerant quantum computation with static linear optics, PRX Quantum **2**, 040353 (2021).

[3] S. Bartolucci, P. Birchall, H. Bombín, H. Cable, C. Dawson, M. Gimeno-Segovia, E. Johnston, K. Kieling, N. Nickerson, M. Pant, F. Pastawski, T. Rudolph, and C. Sparrow, Fusion-based quantum computation, Nat. Commun. **14**, 912 (2023).

[4] K. Alexander *et al.*, A manufacturable platform for photonic quantum computing, Nature (London) **641**, 876 (2025).

[5] B. W. Walshe, B. Q. Baragiola, H. Ferretti, J. Gefaell, M. Vasmer, R. Weil, T. Matsuura, T. Jaeken, G. Pantaleoni, Z. Han, T. Hillmann, N. C. Menicucci, I. Tzitrin, and R. N. Alexander, Linear-optical quantum computation with arbitrary error-correcting codes, Phys. Rev. Lett. **134**, 100602 (2025).

[6] H. Aghaee Rad *et al.*, Scaling and networking a modular photonic quantum computer, Nature (London) **638**, 912 (2025).

[7] H. J. Briegel, D. E. Browne, W. Dür, R. Raussendorf, and M. Van den Nest, Measurement-based quantum computation, Nat. Phys. **5**, 19 (2009).

[8] R. Raussendorf and J. Harrington, Fault-tolerant quantum computation with high threshold in two dimensions, Phys. Rev. Lett. **98**, 190504 (2007).

[9] N. Nickerson and H. Bombín, Measurement based fault tolerance beyond foliation, arXiv:1810.09621.

[10] M. Newman, L. A. de Castro, and K. R. Brown, Generating fault-tolerant cluster states from crystal structures, Quantum **4**, 295 (2020).

[11] A. Bolt, G. Duclos-Cianci, D. Poulin, and T. M. Stace, Foliated quantum error-correcting codes, Phys. Rev. Lett. **117**, 070501 (2016).

[12] B. J. Brown and S. Roberts, Universal fault-tolerant measurement-based quantum computation, Phys. Rev. Res. **2**, 033305 (2020).

[13] A. M. Steane, Error correcting codes in quantum theory, Phys. Rev. Lett. **77**, 793 (1996).

[14] A. R. Calderbank and P. W. Shor, Good quantum error-correcting codes exist, Phys. Rev. A **54**, 1098 (1996).

[15] H. Bombin and M. A. Martin-Delgado, Homological error correction: Classical and quantum codes, J. Math. Phys. **48**, 052105 (2007).

[16] N. P. Breuckmann and J. N. Eberhardt, Quantum low-density parity-check codes, PRX Quantum **2**, 040101 (2021).

[17] M. B. Hastings, Weight reduction for quantum codes, Quantum Inf. Comput. **17**, 1307 (2017).

[18] S. Evra, T. Kaufman, and G. Zémor, Decodable quantum ldpc codes beyond the $\sqrt{n}$ distance barrier using high-dimensional expanders, SIAM J. Comput. **53**, FOCS20-276 (2022).

[19] J.-P. Tillich and G. Zémor, Quantum LDPC codes with positive rate and minimum distance proportional to the square root of the blocklength, IEEE Trans. Inf. Theory **60**, 1193 (2014).

[20] W. Zeng and L. P. Pryadko, Higher-dimensional quantum hypergraph-product codes with finite rates, Phys. Rev. Lett. **122**, 230501 (2019).

[21] E. Dennis, A. Kitaev, A. Landahl, and J. Preskill, Topological quantum memory, J. Math. Phys. **43**, 4452 (2002).

[22] M. Vasmer and D. E. Browne, Three-dimensional surface codes: Transversal gates and fault-tolerant architectures, Phys. Rev. A **100**, 012312 (2019).

[23] A. O. Quintavalle, M. Vasmer, J. Roffe, and E. T. Campbell, Single-shot error correction of three-dimensional homological product codes, PRX Quantum **2**, 020340 (2021).

[24] O. Higgott and N. P. Breuckmann, Improved single-shot decoding of higher-dimensional hypergraph-product codes, PRX Quantum **4**, 020332 (2023).

[25] C. Gidney, Stability experiments: The overlooked dual of memory experiments, Quantum **6**, 786 (2022).

[26] D. Gottesman, Stabilizer codes and quantum error correction, arXiv:quant-ph/9705052.

[27] We note that a similar approach has recently been explored in the context of condensed matter physics [74,75].

[28] C. Gidney, Stim: A fast stabilizer circuit simulator, Quantum **5**, 497 (2021).

[29] P.-J. H. S. Derks, A. Townsend-Teague, A. G. Burchards, and J. Eisert, Designing fault-tolerant circuits using detector error models, arXiv:2407.13826.

[30] D. Gottesman, Opportunities and challenges in fault-tolerant quantum computation, arXiv:2210.15844.

[31] N. Delfosse and A. Paetznick, Spacetime codes of clifford circuits, arXiv:2304.05943.

[32] H. Bombin, C. Dawson, T. Farrelly, Y. Liu, N. Nickerson, M. Pant, F. Pastawski, and S. Roberts, Fault-tolerant complexes, arXiv:2308.07844.

[33] X. Fu and D. Gottesman, Error correction in dynamical codes, arXiv:2403.04163.

[34] M. E. Beverland, S. Huang, and V. Kliuchnikov, Fault tolerance of stabilizer channels, arXiv:2401.12017.

[35] Y. Li, Low-density parity-check representation of fault-tolerant quantum circuits, Phys. Rev. Res. **7**, 013115 (2025).

[36] See Supplemental Material at http://link.aps.org/supplemental/10.1103/cjb4-l57n for details of the results discussed in the main text, and information on the numerical simulations, which includes Refs. [76–84].

[37] R. Raussendorf, S. Bravyi, and J. Harrington, Long-range quantum entanglement in noisy cluster states, Phys. Rev. A **71**, 062313 (2005).

[38] D. Horsman, A. G. Fowler, S. Devitt, and R. V. Meter, Surface code quantum computing by lattice surgery, New J. Phys. **14**, 123011 (2012).

[39] A. G. Fowler and C. Gidney, Low overhead quantum computation using lattice surgery, arXiv:1808.06709.

[40] D. Litinski, A game of surface codes: Large-scale quantum computing with lattice surgery, Quantum **3**, 128 (2019).

[41] H. Bombín, Single-shot fault-tolerant quantum error correction, Phys. Rev. X **5**, 031043 (2015).

[42] E. T. Campbell, A theory of single-shot error correction for adversarial noise, Quantum Sci. Technol. **4**, 025006 (2019).

[43] O. Fawzi, A. Grospellier, and A. Leverrier, Constant overhead quantum fault tolerance with quantum expander codes, Commun. ACM **64**, 106 (2020).

[44] S. Gu, E. Tang, L. Caha, S. H. Choe, Z. He, and A. Kubica, Single-shot decoding of good quantum LDPC codes, Commun. Math. Phys. **405**, 85 (2024).

[45] I. Dinur, M.-H. Hsieh, T.-C. Lin, and T. Vidick, Good quantum LDPC codes with linear time decoders, in *STOC 2023: Proceedings of the 55th Annual ACM Symposium on Theory of Computing, Orlando, FL* (ACM, New York, 2023), pp. 905–918.

[46] A. Leverrier, S. Apers, and C. Vuillot, Quantum XYZ product codes, Quantum **6**, 766 (2022).

[47] P. Panteleev and G. Kalachev, Asymptotically good quantum and locally testable classical LDPC codes, in *STOC 2022: Proceedings of the 54th Annual ACM SIGACT Symposium on Theory of Computing* (Association for Computing Machinery, New York, 2022), pp. 375–388.

[48] N. P. Breuckmann and J. N. Eberhardt, Balanced product quantum codes, IEEE Trans. Inf. Theory **67**, 6653 (2021).

[49] M. B. Hastings, J. Haah, and R. O'Donnell, Fiber bundle codes: Breaking the $n^{1/2}$ polylog(n) barrier for quantum LDPC codes, in *STOC 2021: Proceedings of the 53rd Annual ACM SIGACT Symposium on Theory of Computing* (Association for Computing Machinery, New York, 2021), pp. 1276–1288.

[50] B. J. Brown, N. H. Nickerson, and D. E. Browne, Fault-tolerant error correction with the gauge color code, Nat. Commun. **7**, 12302 (2016).

[51] L. Skoric, D. E. Browne, K. M. Barnes, N. I. Gillespie, and E. T. Campbell, Parallel window decoding enables scalable fault tolerant quantum computation, Nat. Commun. **14**, 7040 (2023).

[52] L. Berent, T. Hillmann, J. Eisert, R. Wille, and J. Roffe, Analog information decoding of bosonic quantum low-density parity-check codes, PRX Quantum **5**, 020349 (2024).

[53] S. Huang and S. Puri, Increasing memory lifetime of quantum low-density parity check codes with sliding-window noisy syndrome decoding, Phys. Rev. A **110**, 012453 (2024).

[54] H. Bombín, C. Dawson, Y.-H. Liu, N. Nickerson, F. Pastawski, and S. Roberts, Modular decoding: Parallelizable real-time decoding for quantum computers, arXiv:2303.04846.

[55] T. R. Scruby, T. Hillmann, and J. Roffe, High-threshold, low-overhead and single-shot decodable fault-tolerant quantum memory, arXiv:2406.14445.

[56] P. Panteleev and G. Kalachev, Degenerate quantum LDPC codes with good finite length performance, Quantum **5**, 585 (2021).

[57] J. Roffe, D. R. White, S. Burton, and E. Campbell, Decoding across the quantum low-density parity-check code landscape, Phys. Rev. Res. **2**, 043423 (2020).

[58] N. P. Breuckmann, K. Duivenvoorden, D. Michels, and B. M. Terhal, Local decoders for the 2d and 4d toric code, Quantum Inf. Comput. **17**, 181 (2017).

[59] N. P. Breuckmann and X. Ni, Scalable neural network decoders for higher dimensional quantum codes, Quantum **2**, 68 (2018).

[60] K. Duivenvoorden, N. P. Breuckmann, and B. M. Terhal, Renormalization group decoder for a four-dimensional toric code, IEEE Trans. Inf. Theory **65**, 2545 (2019).

[61] A. Kubica, The abcs of the color code: A study of topological quantum codes as toy models for fault-tolerant quantum computation and quantum phases of matter, Ph.D. thesis, Caltech, 2018.

[62] M. Vasmer, D. E. Browne, and A. Kubica, Cellular automaton decoders for topological quantum codes with noisy measurements and beyond, Sci. Rep. **11**, 2027 (2021).

[63] A. B. Aloshious and P. K. Sarvepalli, Decoding toric codes on three dimensional simplical complexes, IEEE Trans. Inf. Theory **67**, 931 (2021).

[64] T. R. Scruby and K. Nemoto, Local probabilistic decoding of a quantum code, Quantum **7**, 1093 (2023).

[65] T. Hillmann, L. Berent, A. O. Quintavalle, J. Eisert, R. Wille, and J. Roffe, Localized statistics decoding for quantum low-density parity-check codes, Nat. Commun. **16**, 8214 (2025).

[66] N. Berthusen, J. Dreiling, C. Foltz, J. P. Gaebler, T. M. Gatterman, D. Gresh, N. Hewitt, M. Mills, S. A. Moses, B. Neyenhuis, P. Siegfried, and D. Hayes, Experiments with the four-dimensional surface code on a quantum charge-coupled device quantum computer, Phys. Rev. A **110**, 062413 (2024).

[67] D. Bluvstein *et al.*, Logical quantum processor based on reconfigurable atom arrays, Nature (London) **626**, 58 (2024).

[68] H. Zhou, C. Zhao, M. Cain, D. Bluvstein, C. Duckering, H.-Y. Hu, S.-T. Wang, A. Kubica, and M. D. Lukin, Low-overhead transversal fault tolerance for universal quantum computation, Nature (2025), doi:10.1038/s41586-025-09543-5.

[69] D. Kribs, R. Laflamme, and D. Poulin, Unified and generalized approach to quantum error correction, Phys. Rev. Lett. **94**, 180501 (2005).

[70] D. W. Kribs, R. Laflamme, D. Poulin, and M. Lesosky, Operator quantum error correction, Quantum Inf. Comput. **6**, 382 (2006).

[71] D. Poulin, Stabilizer formalism for operator quantum error correction, Phys. Rev. Lett. **95**, 230504 (2005).
[72] A. Kubica and M. Vasmer, Single-shot quantum error correction with the three-dimensional subsystem toric code, Nat. Commun. **13**, 6272 (2022).
[73] P. Panteleev and G. Kalachev, Quantum LDPC codes with almost linear minimum distance, IEEE Trans. Inf. Theory **68**, 213 (2022).
[74] T. Okuda, A. P. Mana, and H. Sukeno, Anomaly inflow for CSS and fractonic lattice models and dualities via cluster state measurement, SciPost Phys. **17**, 113 (2024).
[75] T. Okuda, A. Parayil Mana, and H. Sukeno, Anomaly inflow, dualities, and quantum simulation of Abelian lattice gauge theories induced by measurements, Phys. Rev. Res. **6**, 043018 (2024).
[76] D. Gottesman, A. Kitaev, and J. Preskill, Encoding a qubit in an oscillator, Phys. Rev. A **64**, 012310 (2001).
[77] B. J. Brown, Conservation laws and quantum error correction: Toward a generalized matching decoder, IEEE BITS Inf. Theory Mag. **2**, 5 (2022).
[78] C. Wang, J. Harrington, and J. Preskill, Confinement-Higgs transition in a disordered gauge theory and the accuracy threshold for quantum memory, Ann. Phys. (N.Y.) **303**, 31 (2003).
[79] J. W. Harrington, Analysis of quantum error-correcting codes: Symplectic lattice codes and toric codes, Ph.D. thesis, California Institute of Technology, 2004.
[80] C. Stahl, Single-shot quantum error correction in intertwined toric codes, Phys. Rev. B **110**, 075143 (2024).
[81] W. Zeng and L. P. Pryadko, Minimal distances for certain quantum product codes and tensor products of chain complexes, Phys. Rev. A **102**, 062402 (2020).
[82] M. L. Liu, N. Tantivasadakarn, and V. V. Albert, Subsystem CSS codes, a tighter stabilizer-to-CSS mapping, and Goursat's lemma, Quantum **8**, 1403 (2024).
[83] A. Bolt, D. Poulin, and T. M. Stace, Decoding schemes for foliated sparse quantum error-correcting codes, Phys. Rev. A **98**, 062302 (2018).
[84] D. Bacon, S. T. Flammia, A. W. Harrow, and J. Shi, Sparse quantum codes from quantum circuits, IEEE Trans. Inf. Theory **63**, 2464 (2017).